Published in final edited form as:
J Mol Biol. 2014 January 23; 426(2): 275–285. doi:10.1016/j.jmb.2013.08.026.

Positional effects of AAN motifs in *rpoS* regulation by sRNAs and Hfq

Yi Peng[1], **Toby J. Soper**[1], and **Sarah A. Woodson**[2,*]

[1]Program in Cellular, Molecular and Developmental Biology and Biophysics, Johns Hopkins University, 3400 N. Charles St., Baltimore, MD 21218 USA

[2]T. C. Jenkins Department of Biophysics, Johns Hopkins University, 3400 N. Charles St., Baltimore, MD 21218 USA

Abstract

The *E. coli* stationary phase transcription factor RpoS is translated in response to small noncoding RNAs (sRNAs), which base pair with the *rpoS* mRNA leader. The bacterial Sm-like protein Hfq anneals sRNAs with their mRNA targets by simultaneously binding the mRNA and sRNA. Intriguingly, Hfq is recruited to the *rpoS* leader via AAN motifs far upstream of the sRNA. SHAPE chemical footprinting showed that the *rpoS* leader is divided into a far upstream domain, an Hfq binding domain, and a downstream inhibitory stem-loop containing the sRNA and ribosome binding sites. To investigate how Hfq promotes sRNA-mRNA base pairing from a distance, the natural AAN Hfq binding site was deleted, and artificial AAN binding sites were inserted at various positions in the *rpoS* leader. All the relocated AAN motifs restored tight Hfq binding *in vitro*, but only insertion at the natural position restored Hfq-dependent sRNA annealing *in vitro* and sRNA regulation of *rpoS* translation *in vivo*. Furthermore, U-rich motifs in the downstream inhibitory domain stabilized the *rpoS* mRNA-Hfq complex and contributed to regulation of *rpoS* expression. We propose that the natural Hfq binding domain is optimal for positive regulation because it recruits Hfq to the mRNA and allows it to act on incoming sRNAs without opening the inhibitory stem-loop when sRNA are absent.

Keywords

RNA-protein interactions; bacterial stress response; translational control; RNA chaperone; 5′ UTR

INTRODUCTION

Bacterial small RNAs regulate mRNA translation in response to environmental stress [1-3]. A large class of sRNAs base pair with target mRNAs, inhibiting or activating translation by blocking or exposing the ribosome binding site [4]. sRNA regulation requires Hfq, an RNA chaperone that facilitates sRNA and mRNA annealing and recruits additional proteins to the sRNA-mRNA complex [5, 6]. Despite much progress in identifying sRNA and Hfq binding sites in mRNAs, the molecular “rules” for activation of translation by sRNAs are not fully understood [5].

*Correspondence to: swoodson@jhu.edu; tel. 410-516-2015; FAX 410-516-7448 .

A well-studied example of positive regulation by sRNAs, *rpoS* encodes an alternative stationary phase sigma factor that mediates the expression of many stress response genes [7]. During exponential growth, translation of the *rpoS* mRNA is inhibited by a stable stem-loop that masks the Shine-Dalgarno sequence [8]. Three *E. coli* sRNAs (DsrA, RprA, and ArcZ) up regulate *rpoS* translation by base pairing with the *rpoS* leader and opening the inhibitory stem, releasing the Shine-Dalgarno sequence for translation initiation [9].

An A-rich $(AAN)_4$ motif upstream of the sRNA target site in *rpoS* is needed for sRNA regulation [10] and for Hfq to facilitate annealing of sRNAs to the *rpoS* mRNA [11, 12]. These AAN motifs, which specifically bind the distal face of Hfq, are frequently found in mRNA targets [13, 14]. By contrast, U-rich sequences present in the body and 3′ tail of many sRNAs interact with the lateral rim and proximal face of Hfq [15, 16]. These distinct sRNA and mRNA binding surfaces on each face of Hfq position their complementary regions to interact with a conserved arginine patch on the rim that acts as the active site for RNA annealing [17]. This arginine patch was proposed to orient sRNAs for base pairing [18] and is needed to catalyze the formation and release of RNA base pairs [17].

In vitro experiments on short, unstructured RNAs showed that Hfq anneals two RNAs most efficiently when bound less than 20 nucleotides away from the target, preferably on the 3′ side [19]. This proximity requirement is partially overcome by secondary structure that brings Hfq site closer to the target.

Intriguingly, Hfq binding sites in bacterial mRNAs vary widely in their proximity to the sRNA binding site, and are found both upstream and downstream of the sRNA. Hfq binds *shiA* and *sodB* mRNAs <20 nucleotides away from the 3′ and 5′ of the sRNA annealing site, respectively [20, 21]. Spot42 targets were also found to have AAN motifs within 14 nt of the target site [22]. By contrast, *flhA* mRNA simultaneously binds Hfq distal and proximal surfaces at a distance of 50 nt and 30 nt to the OxyS sRNA binding site, respectively [23]. The AAN motif in *rpoS* mRNA is ≥ 60 nt upstream of the sRNA binding site. These examples suggest that sequence elements within each mRNA may fine tune interactions between Hfq and the sRNA target region, potentially influencing the regulatory outcome.

Here we show that the location of Hfq binding is important for up-regulation of *rpoS* expression by sRNAs in *E. coli*. Using an improved model of the *rpoS* mRNA secondary structure as a guide, we deleted the natural $(AAN)_4$ and A_6 Hfq binding motifs and introduced artificial A_{18} binding sites at different positions upstream and downstream of the sRNA target site. Though *in vitro* assays showed that Hfq binds A_{18} sequences anywhere in the *rpoS* mRNA, Hfq only supports sRNA regulation *in vivo* when recruited to its original location or a site immediately upstream of the sRNA target site. We propose that the native Hfq binding site is optimal because it can communicate with the downstream inhibitory stem-loop through a flexible hinge between two structural domains of the *rpoS* leader.

RESULTS

The full-length *rpoS* leader forms three domains

A previous model of a 323 nt fragment of the *rpoS* mRNA showed that the single-stranded $(AAN)_4$ Hfq binding motif was imbedded in secondary structure upstream of the inhibitory stem-loop [12]. To better predict how upstream sequences influence *rpoS* translation, we determined the secondary structure of the entire full-length *rpoS* leader using SHAPE to measure the backbone flexibility of individual nucleotide (Fig. 1A) [24, 25]. SHAPE experiments were performed on transcripts starting from the *rpoS* promoter 567 bp upstream of the start codon and ending 30 nucleotides after the start codon. The scaled reactivity of each residue was converted to a pseudo-free energy term, ΔG_{SHAPE}, and imported into the

dynamic programming algorithm in the RNAstructure program to generate a secondary structure model (Fig 1B) [26-28].

As expected, our SHAPE data on the full-length leader was consistent with the regulatory elements identified previously. First, the 3′ end of the leader formed an inhibitory stem-loop between the sRNA annealing site and the Shine-Dalgarno sequence (Fig. 1B), identical to the structure based on genetic data [8] and structure probing of the truncated leader [12, 29]. Second, the upstream $(AAN)_4$ and A_6 motifs that bind the distal face of Hfq were again predicted to reside in two single-stranded regions of the leader, separated by a short helix similar to our previous model [12].

On the other hand, our new model predicted three additional features likely to be important for translational control (Fig. 1B). First, the inhibitory stem was extended by 15 bp due to the base pairing between the upstream of the sRNA annealing site and the coding sequence. This extended base pairing is supported by reduced modification of the 5′ side of the stem (nt 435 – 450); the 3′ side (nt 570-590) is covered by the cDNA primer and was not assayed in our SHAPE experiments. The sRNA target site (nt 446-470) was less modified than the rest of the inhibitory stem, suggesting that base pairs between the sRNA target and the Shine-Dalgarno sequence are more stable than those involving the coding region. The longer inhibitory stem, however, may account for the lower basal expression of *rpoS* mRNAs containing the full-length leader [10].

Second, the hinge region between the inhibitory stem and the upstream AAN motifs was shortened and joined to the far upstream region as a four-way-junction. The moderate SHAPE reactivity of residues just downstream of the four-way-junction indicated that the hinge is dynamic and could allow for tertiary contacts between the upstream and downstream domains.

Third, the far upstream region was predicted to form four extended helices with very low SHAPE reactivity, indicating that the 5′ half of the leader forms a highly stable secondary structure. Thus, the full-length *rpoS* leader can be divided into three domains: the far upstream domain, the A-rich domain containing the strong Hfq binding site, and the downstream inhibitory stem domain. Based on the extent of modification, the A-rich domain and flexible hinge were more dynamic than other regions of the leader.

Ectopic Hfq binding sites rescue *rpoS* regulation in vivo

We next attempted to understand how the functional elements of the *rpoS* leader were organized to interact with Hfq, the regulatory sRNAs, and the translation machinery. Upstream $(AAN)_4$ and A_6 motifs specifically bind the distal face of Hfq and contribute to sRNA regulation [10, 12]. We asked whether the position of the Hfq binding site is important for regulation by relocating A-rich motifs to other regions of the *rpoS* leader.

A double mutant (*rpoSΔ2*) lacking both the $(AAN)_4$ and A_6 motifs cannot bind Hfq tightly, and consequently Hfq no longer facilitates its annealing with the sRNAs [10]. Using our secondary structure model as a guide, we inserted an A_{18} sequence cassette at various positions in the three domains of *rpoSΔ2* (Fig. 2A). Insertion sites chosen for further study were in the far upstream region (positions 53 and 250), the original $(AAN)_4$ loop (position 366), 5′ of the inhibitory stem (position 441), and the 3′ of the sRNA binding site (positions 484, 499, and 519) (Fig. 2A). All of these sites were designed to minimize perturbations to the mRNA structure, as predicted by MFOLD [30]. Partial SHAPE modification data of Δ2-366A18 and Δ2-519A18 RNAs indicated these insertions do not grossly change the secondary structure of the inhibitory domain (data not shown).

To determine whether these ectopic Hfq binding sites could support *rpoS* regulation *in vivo* (Fig. 2B), the *rpoS* leaders were fused to the *lacZ* reading frame in the *E. coli* chromosome as previously described [31]. RpoS translation was induced by overexpression of DsrA, RprA, or ArcZ sRNA (pLac), and expression of the *rpoS-lacZ* fusion was obtained from the specific β-galactosidase activity of cell cultures in the late-log to early-stationary phase.

As expected, *rpoSΔ2-lacZ* fusions lacking the upstream AAN motifs were translated 30% - 50% less than the wild type *rpoS-lacZ* fusion, when DsrA, RprA or ArcZ sRNAs were over-expressed in the presence of IPTG (Fig. 2C, green, yellow and red bars). Basal expression of *rpoSΔ2-lacZ* in the presence of empty vector (pLac) was also 30% lower that for the wild type *rpoS* fusion (Fig. 2C, blue bars), indicating that the AAN motifs are important for activation by endogenous sRNAs. As cells over-expressing DsrA (Fig. 2C, green bars) can induce *rpoS* without Hfq [10], these A_{18} strains were least affected by deletion of the AAN motifs.

We next asked whether A_{18} insertions could rescue Hfq-dependent translation of *rpoSΔ2*. When the A_{18} Hfq binding site was located far upstream in the *rpoS* leader (positions 53 and 250), the expression levels remained the same, suggesting these sites are too far from the sRNA target site. When A_{18} was inserted at the natural location of the $(AAN)_4$ motif (position 366) or 5′ of the sRNA target site (position 441), basal and activated expression improved about 2-fold compared to *rpoSΔ2* (Fig. 2C, Δ2-366A18 and Δ2-441A18), suggesting that activation by endogenous and over-produced sRNAs is restored when Hfq binds near the sRNA target site.

By contrast, A_{18} insertions 3′ of the sRNA target site did not rescue *rpoS* expression (positions 484, 499, and 519). In fact, insertions at positions 484 and 499 decreased the level of expression by half under some conditions (Fig. 2C, Δ2-484A18 and Δ2-499A18). Therefore, the level of expression depended on the position of the A_{18} insertion and was optimal when this sequence was placed just upstream of the sRNA (Fig. 2C).

rpoS regulation requires 5′ Hfq binding in vivo

If the *rpoS*Δ2-A18 fusions rescue expression by recruiting Hfq to the mRNA, then deleting *hfq* from the cells should erase any change of expression induced by A_{18} insertions. We deleted *hfq* from strains containing the *rpoS::lacZ* fusions, and re-measured the ability of sRNAs to activate *rpoS* translation. Deleting *hfq* lowered expression of all the *rpoS* fusions tested (Fig. 2D), apart from strains over-expressing DsrA that do not require Hfq to induce *rpoS* expression [10]. Moreover, the Δ2-366A18 and Δ2-484A18 fusions were expressed at a level similar to the *rpoSΔ2* mutant in the *hfq*$^-$ strains. This indicates that the different activities of the A18-containing leaders arise from their ability to bind Hfq, and not from a difference in the mRNA stability or translation levels.

When A_{18} was inserted at position 441 immediately 5′ of the sRNA binding site, expression was slightly higher even without Hfq. We speculate that this insertion weakens the inhibitory stem-loop, causing leaky repression of translation initiation. None of the *rpoSΔ2*-A18 reporters were as active as the wt *rpoS*::lacZ fusion, possibly because the $(AAN)_4$ deletion alters the structure of the Hfq binding domain [10]. Nonetheless, the ability of A_{18} insertions to partially restore *rpoS* translation in the presence of Hfq suggested that sRNA regulation requires recruitment of Hfq to an AAN binding site within 80 nt upstream of the sRNA.

A_{18} insertion restores tight Hfq binding in vitro

We next analyzed how the A_{18} insertions at different positions affect Hfq binding to the *rpoS* mRNA leader. Based on our structural model of the full-length leader (Fig. 1B), we designed a new 301 nt *rpoS* leader that lacks the far upstream helices (nt 9–300) that are not required for Hfq binding [12], but retains the 5′ fragment (nt 1–8) that forms part of the hinge region. The resulting *rpoS301* leader contained the upstream $(AAN)_4$ and A_6 motifs, the flexible hinge, and the downstream inhibitory stem (Fig. 3A). It migrated as single species in native polyacrylamide gel, indicating more uniform folding than the previous *rpoS323* truncation [10, 12].

We previously found that a 323 nt *rpoS* RNA bound multiple Hfq hexamers in native (TBE) polyacrylamide gels, described by one tight and several nonspecific binding sites with dissociation constants K_T = 0.28 μM and K_{nsp} = 1 μM Hfq monomer [12]. To better discriminate between specific and non-specific Hfq binding, we supplemented the running buffer with 2 mM Mg^{2+} to stabilize the folded RNA. Under these conditions, we observed two specific *rpoS*•Hfq complexes (R•H and R•H2) for WT *rpoS323* (data not shown) and *rpoS301* (Fig. 3B) with dissociation constants K_1 = 0.30 μM and K_2 = 0.42 μM Hfq monomer corresponding to distinct transitions in the Hfq titrations (Fig. 3C). Our model also included a nonspecific binding term (K_{nsp} = 0.87 μM) to account for high molecular weight complexes that did not enter the gel.

The *rpoS301Δ2* RNA, which lacks the upstream AAN motifs, formed only one specific Hfq complex (Fig. 3D), with K_2 = 0.40 μM Hfq monomer (Fig. 3E). Therefore, the Δ2 mutation abolished the strongest Hfq binding site, corresponding to interactions with the $(AAN)_4$ and A_6 motifs (K_1 ~ 0.3 μM Hfq monomer) [12]. The second binding site, K_2 ~ 0.4 μM, also behaved like a specific binding interaction, because it generated a second stable RNP and produced very similar K_d values for wild type and Δ2 *rpoS301*. By contrast, non-specific binding produced high molecular weight complexes that were poorly resolved in these gels. Because low affinity non-specific complexes (0.7–1 μM Hfq) were treated collectively in our partition function, the resulting K_{nsp} values varied considerably among different *rpoS* RNAs.

With our optimized *rpoS301* truncation and improved Hfq titration, we measured Hfq binding constants for all the *rpoSΔ2*-A18 fusions. All the A_{18} insertions restored tight Hfq binding with K_1 values comparable to the wild type *rpoS301* (0.26 to 0.33 μM; Fig. 3F, red bars). Like WT *rpoS*, *rpoSΔ2*-366A18, Δ2-441A18, and Δ2-519A18 formed a second specific complex with K_2 ~ 0.4 μM (Fig. 3F, blue bars, and Fig. S1A, B and E). Surprisingly, the downstream insertions Δ2-484A18, and Δ2-499A18 (Fig. S1C and D) formed the first Hfq complex but not the second complex (Fig. 3F, blue bars). These insertions may disrupt the second binding site, or indirectly disrupt the second RNP by changing the *rpoS* mRNA conformation. In summary, all the A_{18} insertions tested were capable of binding Hfq, showing that recognition is independent of context. However, insertions at positions 484 and 499 in the inhibitory stem-loop domain disrupted a second specific interaction with Hfq.

5′ Hfq binding facilitates DsrA•*rpoS301* annealing in vitro

While Hfq was able to bind A_{18} sequences at any position in the *rpoS* leader, only A_{18} insertions 5′ of the sRNA target sequence rescued sRNA regulation *in vivo*. We next determined whether Hfq must be recruited to a specific location in the *rpoS* leader to facilitate annealing of DsrA sRNA with the *rpoS301* RNA using native gel mobility shift assays. As expected, while WT *rpoS301* annealed with DsrA slowly in the absence of Hfq (Fig. 4A), it rapidly formed a ternary complex with DsrA and 0.6 μM Hfq (Fig. 4B).

Consistent with previous studies [10], the initial annealing rate with Hfq was 2.5 min^{-1}, 62 times faster than with no Hfq (0.04 min^{-1}; Fig. 4C,D). By contrast, *rpoS301*Δ2 was unable to form the ternary complex, and the annealing kinetics was about the same with and without Hfq (0.018 min^{-1} and 0.012 min^{-1}, respectively; Fig. S2A).

We then compared the DsrA annealing kinetics with or without Hfq for all the *rpoS301* RNAs containing A_{18} insertions. All the insertions except Δ2-441A18 had little effect on the annealing rate in the absence of Hfq (ranging from 0.011 to 0.016 min^{-1}), suggesting that the DsrA•*rpoS* mRNA interaction alone was not altered by an A_{18} insertion at most positions (Fig. S2, left column). The Δ2-441A18 RNA was almost unable to base pair with DsrA without Hfq (Fig. S2, C left column), possibly because the insertion at nt 441 changes the *rpoS* mRNA structure (Fig. 3A).

All the A_{18} insertions allowed Hfq to facilitate sRNA annealing to some degree, depending on the location. First, unlike *rpoSΔ2*, they all formed stable ternary complexes with Hfq and DsrA (Fig. S2, middle column), indicating that any A-rich Hfq binding site in the *rpoS* leader was necessary and sufficient for stable ternary complexes. Second, Hfq accelerated DsrA annealing with all the Δ2-A18 RNAs (Fig. S2, right column), but insertions 5′ of the sRNA restored the annealing kinetics to the same level as WT *rpoS*301, while insertions 3′ of the sRNA did not (Fig. 4D). These data agreed with our *in vivo* results, that Hfq promotes sRNA-*rpoS* mRNA interactions most effectively when the AAN motif is placed 5′ of the sRNA annealing site.

Downstream A-/U-rich sequences stabilize *rpoS* mRNA conformation

Interestingly, positions 484, 499, and 519 are each adjacent to short A-/U-rich patches that might interact directly with Hfq or might form tertiary interactions in the *rpoS* leader. We first confirmed whether those A-/U-rich sequences are functionally important by converting them to G-/C-rich sequences (Fig. 2A; Δ484, Δ499, and Δ519), and measuring up regulation of those mutants by Hfq and sRNAs using β-galactosidase assay described above. The Δ484, Δ499, and Δ519 mutations all reduced expression of *rpoS-lacZ* significantly compared to the wild type *rpoS* leader (Fig. 5A). Mutation of the U-rich loop at position Δ484 was the most detrimental, decreasing expression levels by average 40%, followed by Δ519 with expression levels decreased by ~30%, and Δ499 with a moderate 20% decrease of expression levels.

We next tested whether these A-/U-rich sequences were Hfq binding sites. The Δ484, Δ499, and Δ519 mutants all formed two specific Hfq complexes in vitro (Fig. S3, left column), suggesting that both tight and weak Hfq binding sites were retained even though insertions at these positions disrupted the weak complex. All three single mutations weakened Hfq binding overall, however, increasing K_1 from 0.3 μM to 0.45 μM, and K_2 from 0.4 μM to 0.55 μM (Fig. 5B). While we cannot exclude the possibility that the A-/U-rich sequences contact Hfq directly, these data suggested that these loops fold the *rpoS* leader in a manner that favors Hfq recognition.

If our original A_{18} insertions at positions 499 and 519 (Δ2-499A18 and Δ2-519A18) lowered *rpoS* expression by disrupting tertiary interactions formed by the A-/U-rich sequences at those positions, inserting A_{18} into the wild type *rpoS* leader at positions 499 and 519 should cause a similar loss of function. In fact, both wt-499A18 and wt-519A18 showed reduced expression compared to WT *rpoS::lacZ* (Fig. 5A). We found that wt-499A18 was more deleterious than wt-519A18 (60 - 64% and 33% - 57% reduction, respectively), consistent with our results with Δ2-499A18 and Δ2-519A18 (Fig. 2C). Together, these data suggest that the downstream A-/U-rich sequences are important for *rpoS* function because they

stabilize the tertiary conformation of the mRNA and Hfq recognition, and that this accounts for why Hfq binding sites downstream of the sRNA target site reduce *rpoS* up-regulation.

DISCUSSION

Position of the AAN motif in the *rpoS* leader affects Hfq regulation

Most bacterial mRNAs regulated by sRNAs contain AAN motifs that bind Hfq [5]. The upstream (AAN) motifs in the *rpoS* mRNA leader are required for Hfq-dependent regulation of *rpoS* translation by sRNAs in *E. coli* [10] and accelerated sRNA-mRNA base pairing *in vitro* [11, 12]. By relocating the AAN motif within the *rpoS* leader, we found that Hfq recognized this motif at all the positions tested, but Hfq-dependent regulation was only rescued when its binding site was placed close to the 5′ side of the sRNA annealing site. Therefore, the location of Hfq within the *rpoS* leader determines its chaperone function and its ability to act in translational control.

Our study identifies three factors that determine how the position of the AAN motif affects Hfq regulation. First, experiments using short unstructured RNAs showed that Hfq must interact with both the sRNA and mRNA to catalyze the formation of base pairs [17], and is most effective when bound within 20 nt of the sRNA target site [19]. Although the *rpoS* $(AAN)_4$ motif is about 60 nt upstream of the sRNA binding site, our results suggest the flexible hinge allows the Hfq-binding domain to fold back on the inhibitory stem-loop, placing the lateral rim of Hfq where it can engage an incoming sRNA and its mRNA complement. In agreement with this hypothesis, A_{18} insertions far upstream (positions 53 and 250) or far downstream (position 519) of the sRNA binding site did not restore Hfq regulation, suggesting that the necessary tertiary interaction with the inhibitory stem was abolished.

Second, downstream A-/U-rich sequences may help position Hfq to interact with the sRNA binding site. Our results show that A-/U-rich sequences at positions 484 and 499 in the *rpoS* leader contribute to Hfq regulation, as replacing them with A_{18} or mutating them reduced Hfq regulation in vivo and weakened Hfq binding in vitro. The loop at position 484 was protected by Hfq in ribonuclease footprinting experiments on a minimal *rpoS* mRNA and may interact with Hfq directly [29]. These nucleotides may also make RNA interactions that stabilize the overall conformation of the *rpoS* leader.

Third, A_{18} insertions in the inhibitory stem-loop of *rpoS* disturb the balance between translation repression and activation and are thus disadvantageous for sRNA regulation. This was suggested by the observation that the A_{18} insertion at the natural $(AAN)_4$ site (position 366) restored Hfq function better than the A_{18} insertion immediately 5′ of the sRNA binding site (position 441), though in vitro studies predicted the latter should be more effective.

The A_{18} insertion next to the sRNA target site may hinder DsrA base pairing. In agreement with that, Δ2-441A18 barely annealed to DsrA in the absence of Hfq, although Hfq accelerated this reaction almost 60-fold. Additionally, the A_{18} insertion in the inhibitory stem-loop likely destabilizes its secondary structure, as basal expression of rpoS Δ2-441A18 was slightly elevated when DsrA was over-expressed in the *hfq*$^-$ strain (Figure 2D) or in the pLac control in the *hfq*$^+$ strain (Figure 2C). Higher basal translation initiation compensated for the reduced sRNA annealing rate, so that expression of Δ2-441A18 in the wt background was equal to expression of Δ2-366A18.

General implications for Hfq regulation of other mRNAs

In mRNAs regulated by Hfq and sRNAs, the AAN binding motif occurs at various positions with respect to the start of the open reading frame and the binding sites for sRNAs [20-23]. The

three factors discussed above suggest how the structural context of Hfq binding can modulate the efficiency of sRNA regulation in other mRNAs.

First, the optimal location for Hfq likely depends on whether the sRNA increases or decreases expression. In many negatively regulated mRNAs in which the sRNA represses translation by base pairing with the Shine-Dalgarno sequence, Hfq binds near the sRNA target site [32]. Our results predict this proximity between Hfq and the sRNA target maximizes the ability of Hfq to facilitate sRNA annealing [19]. In some cases, Hfq binds so close to the Shine-Dalgarno sequence that Hfq directly competes with ribosome entry [21]. In studies using artificial mRNA and sRNA mimics, a stable Hfq-sRNA-mRNA ternary complex recruits RNase E to the message via interactions with a 5′ monophosphate on the sRNA [33]. Moreover, Hfq was shown to directly recruit RNase E to *ptsG* mRNA for SgrS sRNA mediated degradation [34]. Thus, strong Hfq binding sites near the site of regulation may make translation repression or mRNA turnover more efficient.

On the other hand, positively regulated mRNAs tend to adopt more complicated secondary structures that inhibit translation initiation in the absence of sRNA but open to permit ribosome binding when the sRNA is present [5]. In these examples, Hfq may bind far from the sRNA, in which case it is presumably delivered to the site of the action by the mRNA structure. We found that the *rpoS* leader is organized into distinct domains dedicated to inhibition and Hfq binding. Our results suggest this organization will be generally advantageous for positive control, because Hfq can be recruited to the mRNA without disrupting its inhibitory self-structure. This organization may also allow Hfq to release the sRNA-mRNA double helix once annealing is complete.

Finally, other sequence elements in the mRNA may fine-tune or stabilize Hfq interactions. Downstream A-/U-rich patches in *rpoS* stabilize Hfq binding to the upstream $(AAN)_4$ motif and improve Hfq-dependent regulation, consistent with previous findings that Hfq restructures certain mRNAs [35, 36]. In *flhA* mRNA, a second Hfq binding site was identified that interacted with the proximal face of Hfq and enhanced binding of the distal face to AAN motifs [23]. Alternatively, A-/U-rich patches in the mRNA may help displace the sRNA from the lateral rim of Hfq, where the body of the sRNA has been shown to bind [18]. Though further work is needed to fully understand how Hfq interacts with its mRNA targets, the results presented here demonstrate that the ability of Hfq to act in sRNA regulation depends on its structural context.

MATERIALS AND METHODS

SHAPE footprinting

Full-length *rpoS* leader RNA was renatured by heating to 75 °C for 1 min and cooling to room temperature for 5 min before use. For SHAPE modification, *rpoS* mRNA (0.5 pmol) was combined with 2 μL 5X TNK buffer (50 mM Tris-HCl pH 8.0, 250 mM NaCl, 250 nM KCl), 2 μL 5X Hfq buffer (50 mM Tris–HCl pH 7.5, 1 mM EDTA, 250 mM NH_4Cl) and 2 μL TE in 10 μL total volume and incubated up to 2 hr at 25°C. 1-methyl-7-nitroisatoic anhydride (1M7; 1 μL 5 mM in anhydrous DMSO) was added and allowed to react completely. Reactions were diluted to 200 μL with 0.1 mg/mL carrier tRNA, extracted with phenol and chloroform, the RNA precipitated with ethanol and resuspended in 2 μL water. Modified RNA was analyzed by primer extension with dye-labeled primers as previously described [12, 24] using a Beckman CEQ8000.

Raw CE peaks were assigned and integrated using ShapeFinder [37]. After background subtraction, peak volumes were scaled to the average of the top 10% of values after exclusion of outliers using model free statistics [27]. Data from 7-8 independent experiments

were averaged and the one-sided Grubb's test used to pick single outliers between different experiments. Average SHAPE reactivities (negative numbers were set to zero) were used to constrain secondary structures predicted by RNAstructure [27].

Construction of *rpoS* mutants and A_{18} insertions

The pUC18 plasmids of full-length wt and Δ2 *rpoS* were published previously and were used as templates for generating *rpoS* mutations and A_{18} insertions in this study [10, 12]. The plasmid carrying wt *rpoS* was used to derive Δ484, Δ499, Δ519, wt-499A18, and wt-519A18; the plasmid carrying Δ2 *rpoS* was used to derive Δ2-366A18, Δ2-441A18, Δ2-484A18, Δ2-499A18, and Δ2-519A18. All the constructs were made by inverse PCR as described previously [38]. The primers for generating mutations or insertions are listed in Table S2.

β-Galactosidase assays

Bacterial strains (Table S3) containing chromosomal *rpoS::lacZ* fusions were constructed from strain PM1205 as previously described [10]. DNA fragments for making the recombinant bacterial strains and in vitro transcription were generated by PCR amplification of the corresponding pUC18 plasmids with primers Pbad-rpoS-F and lacZ-rpoS10aa-R (Table S2). The *hfq*$^{-}$ strains were generated by P1 phage transduction [39]. The strains were transformed with pLac, pDsrA, pRprA, or pArcZ plasmids that were previously published [10].

Overnight cultures of transformed cells were diluted 1:500 into fresh LB medium containing ampicillin (100 μg/mL), arabinose (0.2%), and IPTG (100 μM). They were grown at 37°C with 250 rpm agitation for about 4-6 hrs or until their OD_{600} reached 0.6-0.8. The OD_{600} was measured, and the cultures were lysed assayed for β-galactosidase activity as described previously [8]. The reaction velocities were determined using a microplate reader (Molecular Device Thermomax), and the specific activity was calculated as V_{max}/OD_{600}. The V_{max} of each culture was the average of 3 aliquots from the same culture, and the reported specific activity of the strain was the average of at least 3 independent experiments.

RNA Preparation

In vitro transcription templates of *rpoS301* were generated by PCR amplification of the corresponding pUC18 plasmids with primers rpoS301F and rpoS576R (Table S2). The unlabeled RNAs were transcribed with T7 RNA polymerase from the PCR templates described above. The RNAs were purified by denaturing PAGE and recovered by phenol-chloroform extraction and ethanol precipitation, as described previously [40]. The ^{32}P labeled *rpoS301* was transcribed in vitro in the presence of $\alpha^{32}P$-ATP [12, 29] and purified through Chroma spin+ TE-100 columns (Clontech Laboratories).

Hfq Preparation

Wild-type *E.coli* Hfq was overexpressed and harvested as previously described [41]. The cells were homogenized (Avestin EmulsiFlex-C3) in 50 mL lysis buffer (50 mM HEPES pH 7.5, 0.5 M NaCl, 20 mM imidazole, 5% glycerol), followed by 1 hr DNase I treatment on ice. The cell lysate was centrifuged and filtered prior to loading on a prepared 5 mL Hi-Trap Co^{2+} column. The column was washed with 50 mL lysis buffer and 150 mL wash buffer (50 mM HEPES pH 7.5, 1 M NaCl, 20 mM imidazole, 5% glycerol), the eluted with 25 mL wash buffer containing 250 mM imidazole. The eluant was concentrated to 5 mL and dialyzed overnight against 1 L 20 mM HEPES pH 7.5, 100 mM NaCl, 0.5 mM EDTA. The protein sample was loaded on a UNO S6 ion exchange column (Bio-Rad), washed with dialysis buffer at 2 mL/min flow rate for 30 min and eluted with a linear gradient of 0.1 M to

1 M NaCl. The desired fractions were pooled and dialyzed against 1 L of Hfq storage buffer (50 mM Tris-HCl pH 7.5, 1 mM EDTA, 250 mM NH_4Cl, 10% glycerol).

Hfq Binding

The equilibrium binding reactions with Hfq and rpoS301 RNA were assembled as previously described [12]. After 10 min at room temperature, 2 μL aliquots were loaded on a native 6% polyacrylamide gel in 1X THEM2 (66 mM HEPES, 34 mM Tris, 0.1 mM EDTA, 2 mM $MgCl_2$). The fractions of bound *rpoS*, f_{RH}, were quantified as previously described [29] and were fit with a partition function (IGOR Pro, WaveMetrics). For *rpoS* constructs that formed only one specific complex with Hfq, we assumed two unequal independent binding sites

$$f_{RH} = \frac{([Hfq]/K_1)^n}{Q_{RH}} \quad (1a)$$

$$Q_{RH} = 1 + ([Hfq]/K1)^n + \left([Hfq]^2/K_1K_2\right)^n \quad (1b)$$

in which [Hfq] is the concentration of Hfq monomers, K_1 is the dissociation constant of the specific complex, K_2 is the apparent dissociation constant of nonspecific binding, and n is the Hill coefficient. Similarly, for *rpoS* constructs that formed two specific Hfq complexes, R•H and R•H2 fractions were fit to the second and third terms of a partition function assuming three unequal independent binding sites:

$$f_{RH} = \frac{([Hfq]/K_1)^n}{Q_{RH}} \quad (2a)$$

$$f_{RH2} = \frac{\left([Hfq]^2/K_1K_2\right)^n}{Q_{RH}} \quad (2b)$$

$$Q_{RH} = 1 + ([Hfq]/K1)^n + \left([Hfq]^2/K_1K_2\right)^n + \left([Hfq]^3/K_1K_2K_3\right)^n \quad (2c)$$

DsrA annealing

Reactions to measure the annealing kinetics of DsrA and *rpoS301* were assembled as previously described [12], except that the native gel was done in 1X THEM2 buffer as described above. The fractions of bound *rpoS* were quantified as previously described [29] and were fit with either a single or double exponential rate equation (IGOR Pro, WaveMetrics)

$$f_{RD} = f\,(1 - \exp(-k_{obs1}t) \quad (3)$$

$$f_{RD+RDH} = f_1\,(1 - \exp(-k_{obs1}t) + f_2\,(1 - \exp(-k_{obs2}t) \quad (4)$$

in which f , f_1, and f_2 are the fractions of the reaction that followed the corresponding annealing rate, t is the annealing time, k_{obs1} is the apparent annealing rate for the slow phase reaction, k_{obs2} is the apparent annealing rate for the fast phase reaction.

Supplementary Material

Refer to Web version on PubMed Central for supplementary material.

Acknowledgments

The authors thank S. Panja for Hfq purification, and N. Majdalani and S. Gottesman for assistance and bacterial strains. This work was supported by a grant from the National Institute of General Medicine (R01 GM46686) to S.W.

REFERENCES

1. Benjamin JA, Desnoyers G, Morissette A, Salvail H, Masse E. Dealing with oxidative stress and iron starvation in microorganisms: an overview. Can. J. Physiol. Pharmacol. 2010; 88:264–272. [PubMed: 20393591]
2. Mandin P, Gottesman S. Integrating anaerobic/aerobic sensing and the general stress response through the ArcZ small RNA. EMBO J. 2010; 29:3094–3107. [PubMed: 20683441]
3. Gerstle K, Klatschke K, Hahn U, Piganeau N. The small RNA RybA regulates key-genes in the biosynthesis of aromatic amino acids under peroxide stress in E. coli. RNA Biol. 2012; 9:458–468.
4. Gottesman S, Storz G. Bacterial small RNA regulators: versatile roles and rapidly evolving variations. Cold Spring Harb Perspect. Biol. 2011; 3 10.1101/cshperspect.a003798.
5. Vogel J, Luisi BF. Hfq and its constellation of RNA. Nat. Rev. Microbiol. 2011; 9:578–589. [PubMed: 21760622]
6. Sobrero P, Valverde C. The bacterial protein Hfq: much more than a mere RNA-binding factor. Crit. Rev. Microbiol. 2012; 38:276–299. 10.3109/1040841X.2012.664540; 10.3109/1040841X.2012.664540. [PubMed: 22435753]
7. Hengge-Aronis R. Stationary phase gene regulation: what makes an Escherichia coli promoter sigmaS-selective? Curr. Opin. Microbiol. 2002; 5:591–595. [PubMed: 12457703]
8. Majdalani N, Cunning C, Sledjeski D, Elliott T, Gottesman S. DsrA RNA regulates translation of RpoS message by an anti-antisense mechanism, independent of its action as an antisilencer of transcription. Proc. Natl. Acad. Sci. U. S. A. 1998; 95:12462–12467. [PubMed: 9770508]
9. Battesti A, Majdalani N, Gottesman S. The RpoS-mediated general stress response in Escherichia coli. Annu. Rev. Microbiol. 2011; 65:189–213. [PubMed: 21639793]
10. Soper T, Mandin P, Majdalani N, Gottesman S, Woodson SA. Positive regulation by small RNAs and the role of Hfq. Proc. Natl. Acad. Sci. U. S. A. 2010; 107:9602–9607. [PubMed: 20457943]
11. Updegrove T, Wilf N, Sun X, Wartell RM. Effect of Hfq on RprA-rpoS mRNA pairing: Hfq-RNA binding and the influence of the 5′ rpoS mRNA leader region. Biochemistry. 2008; 47:11184–11195. [PubMed: 18826256]
12. Soper TJ, Woodson SA. The rpoS mRNA leader recruits Hfq to facilitate annealing with DsrA sRNA. RNA. 2008; 14:1907–1917. 10.1261/rna.1110608; 10.1261/rna.1110608. [PubMed: 18658123]
13. Mikulecky PJ, Kaw MK, Brescia CC, Takach JC, Sledjeski DD, Feig AL. Escherichia coli Hfq has distinct interaction surfaces for DsrA, rpoS and poly(A) RNAs. Nat. Struct. Mol. Biol. 2004; 11:1206–1214. [PubMed: 15531892]
14. Link TM, Valentin-Hansen P, Brennan RG. Structure of Escherichia coli Hfq bound to polyriboadenylate RNA. Proc. Natl. Acad. Sci. U. S. A. 2009; 106:19292–19297. [PubMed: 19889981]
15. Schumacher MA, Pearson RF, Moller T, Valentin-Hansen P, Brennan RG. Structures of the pleiotropic translational regulator Hfq and an Hfq-RNA complex: a bacterial Sm-like protein. EMBO J. 2002; 21:3546–3556. [PubMed: 12093755]
16. Sauer E. Structure and RNA-binding properties of the bacterial Lsm protein Hfq. RNA Biol. 2013; 10:610–618. [PubMed: 23535768]
17. Panja S, Schu DJ, Woodson SA. Conserved arginines on the rim of Hfq catalyze base pair formation and exchange. Nucleic Acids Res. 2013 10.1093/nar/gkt521.

18. Sauer E, Schmidt S, Weichenrieder O. Small RNA binding to the lateral surface of Hfq hexamers and structural rearrangements upon mRNA target recognition. Proc. Natl. Acad. Sci. U. S. A. 2012; 109:9396–9401. [PubMed: 22645344]
19. Panja S, Woodson SA. Hfq proximity and orientation controls RNA annealing. Nucleic Acids Res. 2012; 40:8690–8697. [PubMed: 22761405]
20. Masse E, Gottesman S. A small RNA regulates the expression of genes involved in iron metabolism in Escherichia coli. Proc. Natl. Acad. Sci. U. S. A. 2002; 99:4620–4625. [PubMed: 11917098]
21. Prevost K, Salvail H, Desnoyers G, Jacques JF, Phaneuf E, Masse E. The small RNA RyhB activates the translation of shiA mRNA encoding a permease of shikimate, a compound involved in siderophore synthesis. Mol. Microbiol. 2007; 64:1260–1273. [PubMed: 17542919]
22. Beisel CL, Updegrove TB, Janson BJ, Storz G. Multiple factors dictate target selection by Hfq-binding small RNAs. EMBO J. 2012; 31:1961–1974. [PubMed: 22388518]
23. Salim NN, Feig AL. An upstream Hfq binding site in the fhlA mRNA leader region facilitates the OxyS-fhlA interaction. PLoS One. 2010; 5:e13028. doi: 10.1371/journal.pone.0013028. [PubMed: 20927406]
24. Wilkinson KA, Merino EJ, Weeks KM. Selective 2′-hydroxyl acylation analyzed by primer extension (SHAPE): quantitative RNA structure analysis at single nucleotide resolution. Nat. Protoc. 2006; 1:1610–1616. [PubMed: 17406453]
25. Mitra S, Shcherbakova IV, Altman RB, Brenowitz M, Laederach A. High-throughput single-nucleotide structural mapping by capillary automated footprinting analysis. Nucleic Acids Res. 2008; 36:e63. [PubMed: 18477638]
26. Merino EJ, Wilkinson KA, Coughlan JL, Weeks KM. RNA structure analysis at single nucleotide resolution by selective 2′-hydroxyl acylation and primer extension (SHAPE). J. Am. Chem. Soc. 2005; 127:4223–4231. [PubMed: 15783204]
27. Deigan KE, Li TW, Mathews DH, Weeks KM. Accurate SHAPE-directed RNA structure determination. Proc. Natl. Acad. Sci. U. S. A. 2009; 106:97–102. [PubMed: 19109441]
28. Low JT, Weeks KM. SHAPE-directed RNA secondary structure prediction. Methods. 2010; 52:150–158. [PubMed: 20554050]
29. Lease RA, Woodson SA. Cycling of the Sm-like protein Hfq on the DsrA small regulatory RNA. J. Mol. Biol. 2004; 344:1211–1223. [PubMed: 15561140]
30. Zuker M. Mfold web server for nucleic acid folding and hybridization prediction. Nucleic Acids Res. 2003; 31:3406–3415. [PubMed: 12824337]
31. Mandin P, Gottesman S. A genetic approach for finding small RNAs regulators of genes of interest identifies RybC as regulating the DpiA/DpiB two-component system. Mol. Microbiol. 2009; 72:551–565. [PubMed: 19426207]
32. De Lay N, Schu DJ, Gottesman S. Bacterial small RNA-based negative regulation: Hfq and its accomplices. J. Biol. Chem. 2013; 288:7996–8003. [PubMed: 23362267]
33. Bandyra KJ, Said N, Pfeiffer V, Gorna MW, Vogel J, Luisi BF. The seed region of a small RNA drives the controlled destruction of the target mRNA by the endoribonuclease RNase E. Mol. Cell. 2012; 47:943–953. [PubMed: 22902561]
34. Ikeda Y, Yagi M, Morita T, Aiba H. Hfq binding at RhlB-recognition region of RNase E is crucial for the rapid degradation of target mRNAs mediated by sRNAs in Escherichia coli. Mol. Microbiol. 2011; 79:419–432. [PubMed: 21219461]
35. Geissmann TA, Touati D. Hfq, a new chaperoning role: binding to messenger RNA determines access for small RNA regulator. EMBO J. 2004; 23:396–405. [PubMed: 14739933]
36. Soper TJ, Doxzen K, Woodson SA. Major role for mRNA binding and restructuring in sRNA recruitment by Hfq. RNA. 2011; 17:1544–1550. [PubMed: 21705431]
37. Vasa SM, Guex N, Wilkinson KA, Weeks KM, Giddings MC. ShapeFinder: a software system for high-throughput quantitative analysis of nucleic acid reactivity information resolved by capillary electrophoresis. RNA. 2008; 14:1979–1990. [PubMed: 18772246]
38. Sambrook J, Russell DW. Inverse PCR. CSH Protoc. 2006; 2006:10–1101.
39. Moore SD. Assembling new Escherichia coli strains by transduction using phage P1. Methods Mol. Biol. 2011; 765:155–169. [PubMed: 21815092]

40. Zaug AJ, Grosshans CA, Cech TR. Sequence-specific endoribonuclease activity of the Tetrahymena ribozyme: enhanced cleavage of certain oligonucleotide substrates that form mismatched ribozyme-substrate complexes. Biochemistry. 1988; 27:8924–8931. [PubMed: 3069131]

41. Zhang A, Wassarman KM, Ortega J, Steven AC, Storz G. The Sm-like Hfq protein increases OxyS RNA interaction with target mRNAs. Mol. Cell. 2002; 9:11–22. [PubMed: 11804582]

Highlights

- Regulation of *rpoS* translation by sRNAs requires an AAN binding site for Hfq protein
- The Hfq binding domain is structurally distinct from the translation control domain
- The AAN binding site was relocated to 7 new positions in the *rpoS* mRNA
- Hfq enables sRNA regulation in *E. coli* and in vitro only when bound 5′ of the sRNA
- Structural context of Hfq binding determines the efficiency of sRNA regulation

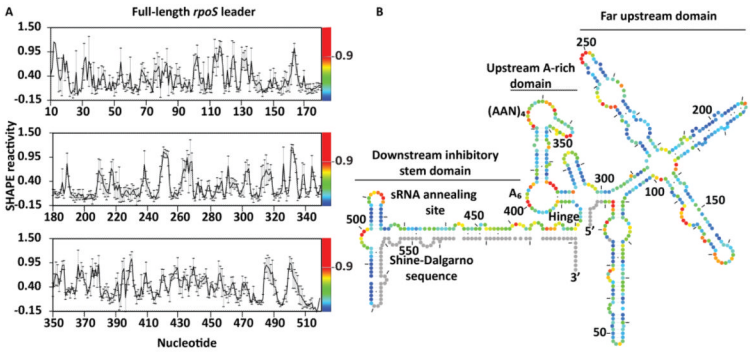

Figure 1. Structural model of the full-length *rpoS* leader

(*A*) Normalized SHAPE reactivity of individual nucleotides, showing the average modification (black line) and standard deviation (error bars) for at least three independent trials. The relative reactivity is represented in the spectrum from red (more reactive) to blue (less reactive). (*B*) Secondary structure of the full-length *rpoS* leader predicted by RNAstructure using SHAPE modification as an energy constraint. Colors as in (A). Grey circles represent 5′ and 3′ sequences that were not mapped in our experiments. The far upstream, A-rich and inhibitory stem-loop domains are indicated. The hinge refers to the flexible helix that connects the A_6 loop and the inhibitory stem.

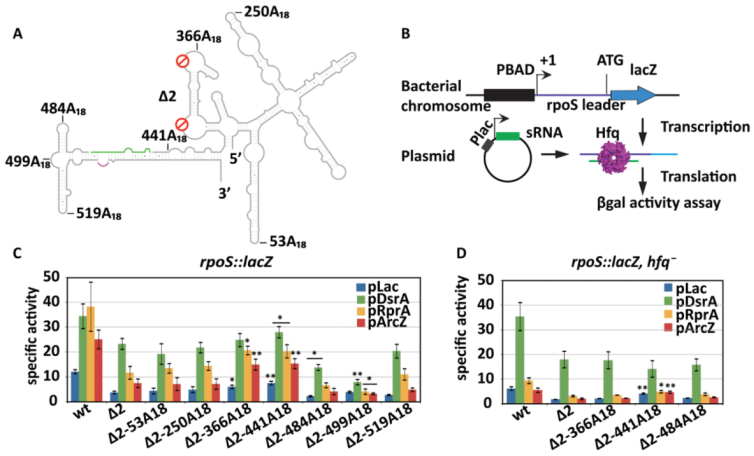

Figure 2. Hfq location determines *rpoS* translational activation *in vivo*

(*A*) Schematic representation of A_{18} insertions in the full-length *rpoS* leader lacking both A-rich motifs (Δ2). The positions are numbered from the *rpoS* transcription start site. The sRNA annealing site, green; Shine-Dalgarno, purple. (*B*) Experimental design. The *rpoS* leader sequence (606 nt) was fused with a chromosomal *lacZ* downstream of a P_{BAD} promoter. DsrA, RprA, or ArcZ sRNA was overexpressed from the P_{lac} promoter on plasmids. Hfq was expressed from its endogenous gene. (*C*) sRNA activation of *rpoS-lacZ* translation. Specific activity of β-galactosidase in strains carrying the *rpoS-lacZ* fusion listed below the x-axis, and transformed with the control plasmid pLac (blue), or plasmids overexpressing DsrA (green), RprA (yellow), and ArcZ (red). Error bars represent the standard deviation of three independent trials. Strains carrying Δ2-A18-*lacZ* fusions were compared to the one carrying Δ2-*lacZ* fusions for their specific activities by unpaired one-tail T-test. Significantly different expression level is marked as * ($p < 0.05$) or ** ($p < 0.01$). Expression levels of all the mutants were significantly lower than wt with $p < 0.01$. (*D*) sRNA activation of *rpoS-lacZ* fusions in an *hfq*$^{-}$ background. Same as in C. Mutant *rpoS-lacZ* fusions were compared to wt *rpoS-lacZ* fusion by unpaired one-tail T-test; * ($p < 0.05$) or ** ($p < 0.01$).

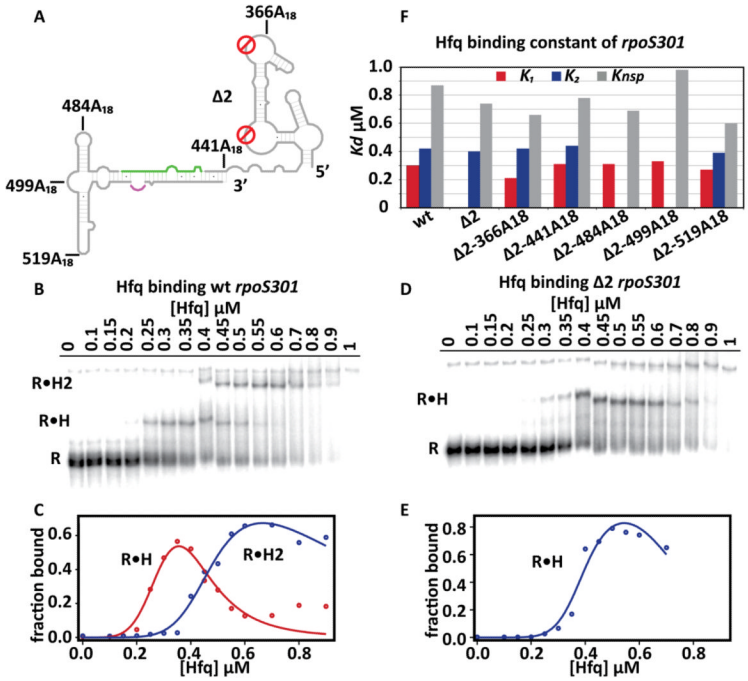

Figure 3. Hfq binds *rpoS* mRNA with A_{18} insertions

(*A*) Schematic representation of the *rpoS301* leader that lacks the far upstream domain. (*B*) Hfq titrations of uniformly labeled wt *rpoS301* at 25°C. Free *rpoS* (R) binds one or two Hfq multimers (R•H and R•H2). A smear of complexes at the top of the gel in high Hfq are not shown. Around 1% of the *rpoS*301 formed a slow migrating band that did not bind Hfq. (*C*) Fraction of bound wt *rpoS301* as a function of [Hfq] was fit to eq. 2 (Methods). Red, R•H (k_1); blue, R•H2 (k_2). The fraction of R•H and R•H2 decreased at high [Hfq] due to formation of high molecular weight (non-specific) complexes. (*D*,*E*) Hfq titrations of uniformly labeled *rpoS301* Δ2 at 25°C as in B and C, except data were fit to eq. 1. (*F*) Comparison of the Hfq binding constants among *rpoS301* wt, Δ2, and Δ2-A18 fusions. Data for Δ2-A18 fusions are shown in Fig. S1; K_d values are listed in Table S1. For *rpoS301* wt, S.D. < 0.02 μM (7%) among 3+ trials.

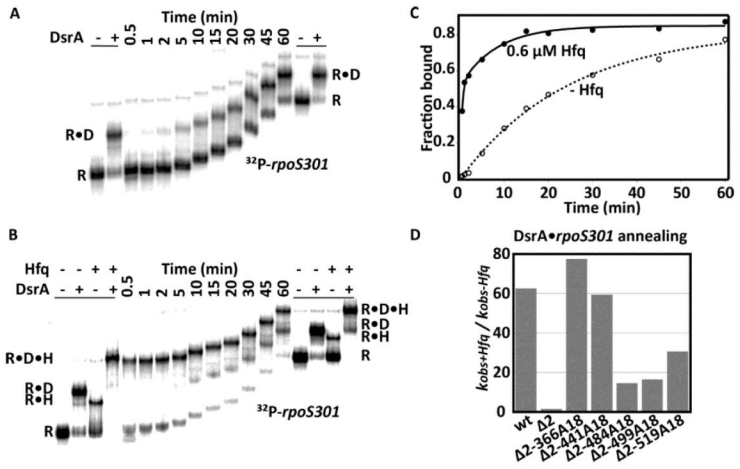

Figure 4. Upstream A_{18} insertions rescue sRNA annealing by Hfq

(*A*) 200 nM DsrA with uniformly labeled wt *rpoS301* without Hfq at 25°C over 60 min. Markers of R and R•D complexes were generated by incubating the same annealing reaction at 25°C for 2 hrs and were loaded before the first time point or after the last time point. (*B*) 200 nM DsrA binding to uniformly labeled wt *rpoS301* with 0.6 μM Hfq as in B, with four markers showing R, R•D, R•H, and R•D•H complexes. Free *rpoS301* migrated as multiple bands 0.5 min after the reaction started, which was not observed in B and may reflect a transient conformational change upon addition of Hfq. (*C*) Binding kinetics of *rpoS* and DsrA in the absence (open circles) and presence of Hfq (closed circles). No Hfq, $k_{obs\text{-}Hfq}$ = 0.04 min^{-1} (82.6%); 0.6 μM Hfq, combined R•D and R•D•H complexes formed with a fast phase *kobs+Hfq* = 2.50 min^{-1} (52 %) and slow phase *kobs+Hfq* = 0.12 min^{-1} (33%). (*D*) DsrA annealing rates of wt, Δ2, and Δ2-A18 *rpoS301* RNAs reported as the ratio of the fast phase *kobs+Hfq* and $k_{obs\text{-}Hfq}$. Data for Δ2 and Δ2-A18 insertions are shown in Fig. S2; rate constants are listed in Table S1.

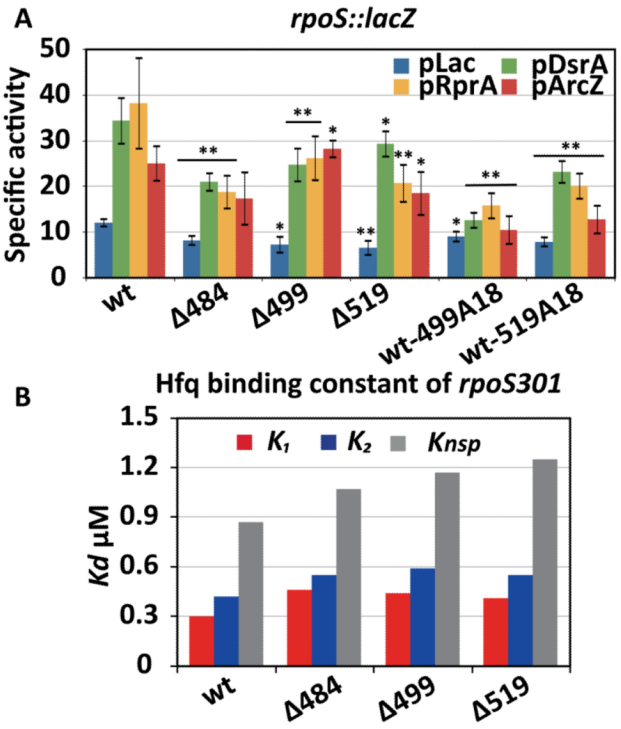

Figure 5. Downstream A-/U-rich motifs contribute to regulation of *rpoS* translation

(*A*) sRNA activation of *rpoS*::*lacZ* fusions *in vivo*, as in Fig. 2C. Hairpin loops at the positions indicated were changed to C-/G-rich sequences, in the wt *rpoS* background. Significantly different expression of mutants from the wt rpoS-lacZ fusion is marked as * ($p < 0.05$) or ** ($p < 0.01$). (*B*) Hfq binding to wt and mutated *rpoS301* RNAs was measured as in Figure 3 and fit to eq. 2 as shown in Fig. S3.